

## Metastability of dark snoidal-type waves in quadratic nonlinear media

Yaroslav V. Kartashov,<sup>1,2</sup> Alexey A. Egorov,<sup>2</sup> Anna S. Zelenina,<sup>2</sup> Victor A. Vysloukh,<sup>3</sup> and Lluís Torner<sup>1</sup>

<sup>1</sup>*ICFO–Institut de Ciències Fòtiques and Department of Signal Theory and Communications, Universitat Politècnica de Catalunya, 08034 Barcelona, Spain*

<sup>2</sup>*Physics Department, M. V. Lomonosov Moscow State University, 119899, Moscow, Russia*

<sup>3</sup>*Departamento de Física y Matemáticas, Universidad de las Américas–Puebla, Santa Catarina Martir, 72820, Puebla, Cholula, Mexico*  
(Received 14 July 2003; published 23 October 2003)

We report the existence and basic properties of dark snoidal-type waves self-sustained in quadratic nonlinear media. Using a stability analysis technique, we reveal that they are almost completely stable, or metastable, in suitable ranges of input energy flows and material parameters. This opens the way to the experimental observation of dark-type multicolor periodic wave patterns supported by quadratic nonlinearities.

DOI: 10.1103/PhysRevE.68.046609

PACS number(s): 42.65.Tg, 42.65.Jx, 42.65.Wi

The possibility of generation of multicolor dark-type soliton light patterns in quadratic nonlinear media has been explored since the early days of the field. A number of dark-type soliton solutions, including multihole, mixed dark-bright, and embedded solutions, are known to exist (see Refs. [1–7]; for reviews, see [8,9]). Most of such solutions have been shown to be highly unstable under evolution, due to the development of both dynamical and modulational instabilities. However, the study of the existence and stability of all possible dark-type solutions is far from complete, and the potential elucidation of stable, or at least metastable, general multicolor dark-type states is an important question that remains open. In this regard, some dark-type solutions could have oscillating tails and hence bound states of a few dark solitons could be formed due to mutual trapping in positions corresponding to the local minima of the effective interaction potential. Such bound states of several dark solitons could be considered as “dark soliton molecules.” A fascinating implementation of this concept is the realization of stable, or metastable, periodic dark-type soliton arrays, and some efforts have been made to find analytical expressions for special bright and dark soliton arrays in quadratic media with the aid of direct substitution [10], Hamiltonian formalisms [11], and Lie-group theoretical methods [12]. However, the construction of complete families of periodic solutions in quadratic media usually requires numerical methods. We recently reported the existence and fundamental properties of such whole families of stationary cnoidal-type and dnoidal-type bright soliton arrays in quadratic nonlinear media. Our numerical simulations revealed that the bright cnoidal wave arrays with high contrasts seem to be robust enough to be observed experimentally [13]. Actually, a rigorous linear stability analysis predicted that completely stable bright cnoidal-wave arrays do exist above a certain threshold energy level [14], thus yielding an example of stable periodic wave patterns in uniform media supporting bright soliton solutions. This provides a renewed motivation to explore the possibility of finding self-sustained stabilized dark-type patterns.

The aim of this paper is to present the properties of dark sn-type periodic waves in  $\chi^{(2)}$  media and to report the outcome of a comprehensive stability analysis based on a powerful technique developed to elucidate the stability of general

periodic nonlinear waves. We show that quadratic nonlinearities admit the existence of continuous families of dark periodic waves with different functional shapes and contrast, and discuss their basic properties. The central result reported is that the linear stability analysis demonstrates that, under appropriate conditions, such waves *do not exhibit exponentially growing instabilities*. Instead, we found that they exhibit only weak small-scale oscillatory instabilities. The weakness of the instabilities is verified by direct numerical simulations of the full dynamical wave evolution. Therefore, we found by numerical simulations that such snoidal-type waves are robust enough to be observed experimentally.

For concreteness, we consider the case of pulsed light propagation in a quadratic nonlinear crystal under conditions of second-harmonic generation, where a fundamental frequency (FF) wave and its second harmonic (SH) interact with each other. The propagation of the corresponding slowly varying envelopes under conditions for noncritical type I phase-matching is described by the system of coupled, reduced equations

$$\begin{aligned} i \frac{\partial q_1}{\partial \xi} &= \frac{d_1}{2} \frac{\partial^2 q_1}{\partial \eta^2} - q_1^* q_2 \exp(-i\beta\xi), \\ i \frac{\partial q_2}{\partial \xi} &= \frac{d_2}{2} \frac{\partial^2 q_2}{\partial \eta^2} - q_1^2 \exp(i\beta\xi). \end{aligned} \quad (1)$$

Here  $q_1 = L_{\text{dis1}}(L_{\text{nl1}}L_{\text{nl2}}/2)^{-1/2}A_1I_0^{-1/2}$  and  $q_2 = (L_{\text{dis1}}/L_{\text{nl1}})A_2I_0^{-1/2}$  are dimensionless complex amplitudes of the fundamental ( $\omega = \omega_0$ ) and second harmonic ( $\omega = 2\omega_0$ ) waves,  $A_{1,2}(\eta, \xi)$  are the slowly varying amplitudes;  $\eta = (t - z/u_{\text{gr1}})/\tau_0$  is the normalized running time;  $u_{\text{gr1}} = (\partial k / \partial \omega)_{\omega = \omega_0}^{-1}$  is the group velocity of the fundamental wave,  $\tau_0$  is the characteristic pulse duration;  $\xi = z/L_{\text{dis1}}$  is the normalized propagation distance;  $L_{\text{dis1,2}} = \tau_0^2 / |\partial^2 k_{1,2} / \partial \omega^2|$  are dispersion lengths;  $k_1 = k(\omega_0)$  and  $k_2 = k(2\omega_0)$  are the wave numbers;  $L_{\text{nl1}} = c^2 k_1 / 4\pi\omega_0^2 I_0^{1/2} \chi^{(2)}(\omega_0)$  and  $L_{\text{nl2}} = c^2 k_2 / 4\pi\omega_0^2 I_0^{1/2} \chi^{(2)}(2\omega_0)$  are nonlinear lengths;  $d_1 = \text{sgn}(\partial^2 k_1 / \partial \omega^2)$  and  $d_2 = \text{sgn}(\partial^2 k_2 / \partial \omega^2)L_{\text{dis1}}/L_{\text{dis2}}$  are the group-velocity dispersion coefficients;  $\beta = \text{sgn}(2k_1 - k_2)L_{\text{dis1}}/L_{\text{coh}}$  is the phase mismatch;  $L_{\text{coh}} = 1/|2k_1 - k_2|$  is the coherence length. We neglect the group-velocity walk-off and assume propagation in near-phase-matched configurations.

The stationary solutions of Eqs. (1) have the form  $q_{1,2}(\xi, \eta) = w_{1,2}(\eta)\exp(ib_{1,2}\xi)$ , where  $w_{1,2}(\eta)$  are real functions and  $b_{1,2}$  are real propagation constants that satisfy  $b_2 = \beta + 2b_1$ . The resulting system of equations for  $w_{1,2}(\eta)$  takes the well-known form

$$\begin{aligned} \frac{d_1}{2} \frac{d^2 w_1}{d\eta^2} + b_1 w_1 - w_1 w_2 &= 0, \\ \frac{d_2}{2} \frac{d^2 w_2}{d\eta^2} + (\beta + 2b_1) w_2 - w_1^2 &= 0, \end{aligned} \quad (2)$$

which, in contrast to the case of fully localized soliton solutions, in the case of sn waves must be solved together with periodic boundary conditions.

It is well known that Eqs. (2) take a simpler form in the large phase-mismatch limit, when  $|\beta| \gg 1$  and the field amplitudes are such that there is a negligible conversion between the fundamental wave and second harmonic. Using the substitution  $w_2(\eta) = w_1^2(\eta)/(\beta + 2b_1)$  for the SH field, one arrives at the approximate equation with cubic nonlinearity

$$\frac{d^2 w_1}{d\eta^2} + \frac{2b_1}{d_1} w_1 - \frac{2}{d_1(\beta + 2b_1)} w_1^3 = 0. \quad (3)$$

Equation (3) has a specific periodic solution in the form of a so-called *snoidal* wave  $w_1(\eta) = m[d_1(2b_1 + \beta)]^{1/2} \text{sn}(\eta, m)$ , where  $m = (2b_1/d_1 - 1)^{1/2}$  is the Jacobi parameter. This solution is valid for the following range of parameters:  $d_1 \geq b_1 \geq d_1/2$  and  $2b_1 + \beta > 0$ , provided that  $d_1 > 0$  and  $\beta > -2d_1$ . The period  $T$  of the snoidal (or sn) wave amounts to  $4K(m)$ , where  $K(m)$  is the elliptic integral of the first kind which grows rapidly as  $m \rightarrow 1$ . In the limit of strong localization ( $m \rightarrow 1$ ) the snoidal wave transforms into an array of out-of-phase dark solitons, while for weak localization ( $m \rightarrow 0$ ) the sn wave transforms into a small amplitude sinusoidal wave.

From now on, we will assume material and pump light conditions such that the FF lies in the normal dispersion region, while the SH frequency lies in the anomalous dispersion region. For simplicity we set equal dispersion lengths for both frequencies and set  $d_1 = 1$ ,  $d_2 = -1$ .

The whole families of periodic solutions of Eqs. (2) could be obtained only numerically, for example, using a relaxation method. The explicit analytical solution in the form of a snoidal wave serves as a good initial guess for the iterative procedure. Despite the fact that the exact solutions of Eqs. (2) at finite phase mismatches  $\beta$  are not described by Jacobi elliptic functions of sn type, by analogy, we will call them *snoidal waves*. The snoidal wave families of Eqs. (2) are defined by two parameters, namely, the transverse period  $T$  and the propagation constant  $b_1$ , for a fixed value of the phase mismatch  $\beta$ . Physically  $b_1$  is related to the energy flow  $U = \int_{-T/2}^{T/2} (w_1^2 + w_2^2) d\eta$  inside each transverse wave period. Since one can use scaling transformations to obtain snoidal waves with different periods from a given family, we select the time scale  $\tau_0$  in such a way that the period  $T$  equals  $2\pi$ , and vary the propagation constant.

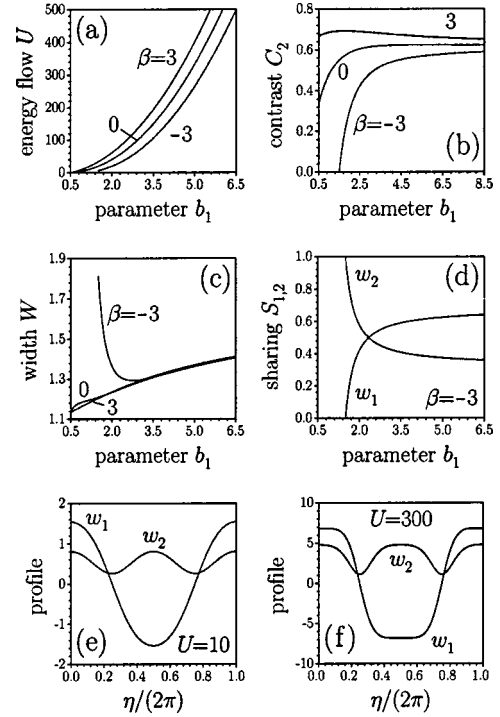


FIG. 1. (a) Dispersion curves for various phase mismatches. Wave contrast (b), integral width (c), and energy sharing (d) versus propagation constant for various phase mismatches. (e) and (f) show snoidal wave profiles with different energy flows at  $\beta = 0$ .

The basic properties of the sn-type waves are summarized in Fig. 1. The dispersion curves  $U(b_1)$  are shown in Fig. 1(a) for different phase mismatches  $\beta$ . There are cutoff values for the propagation constant at different phase mismatches. Thus, for  $-1 \leq \beta < \infty$  one has  $b_1 \geq 1/2$  and both FF and SH waves disappear as  $b_1 \rightarrow 1/2$ , while for  $\beta < -1$ , propagation constant  $b_1 \geq -\beta/2$ , and  $w_1 \rightarrow 0$ ,  $w_2 \rightarrow -(1 + \beta)/2$  at the cutoff point. Among the important characteristics of the dark periodic waves is the contrast

$$C_{1,2} = \frac{|w_{1,2}|_{\max} - |w_{1,2}|_{\min}}{|w_{1,2}|_{\max} + |w_{1,2}|_{\min}}, \quad (4)$$

which is directly related to the amplitude of the constant background, and hence to the potential stability or instability of dark waves. The closer the contrast to 1, the smaller is the amplitude of the constant background. Notice that the FF wave does not contain constant background and thus  $C_1 \equiv 1$  always; thus in Fig. 1(b) we show only the contrast for the SH wave. At  $\beta > 0$  the contrast  $C_2$  varies only slightly, whereas for  $\beta < 0$  it rapidly grows near the cutoff point and saturates to a constant limit with increase of the propagation constant (or energy flow). Notice that the higher the phase mismatch, the higher the contrast. Figure 1(c) shows the integral width

$$W = 2 \left( \int_{-T/4}^{T/4} (w_1^2 + w_2^2) \eta^2 d\eta \right)^{1/2} \left( \int_{-T/4}^{T/4} (w_1^2 + w_2^2) d\eta \right)^{-1/2} \quad (5)$$

versus propagation constant. The slow growth of the integral width with the increase of the energy flow is an indication that dark intensity holes become narrower for high-energy snoidal waves. Notice that the integral width is almost independent of the value of the phase mismatch at high energy flows. The energy sharing per period,

$$S_{1,2} = \frac{1}{U} \int_{-T/2}^{T/2} w_{1,2}^2 d\eta, \quad (6)$$

between the FF and the SH waves is shown in Fig. 1(d) as a function of  $b_1$  for one particular case, at negative phase mismatch. At low energy levels and negative phase mismatches the main part of the energy is concentrated in the SH wave, whereas at high energies  $S_1$  is higher than  $S_2$ . In the case of positive mismatch the FF wave always contains most of the total energy. All this is similar to the general features of quadratic solitons of different types. Typical profiles of the dark periodic waves are displayed in Figs. 1(e) and 1(f) for the low- and high-energy cases, respectively. Notice that snoidal-type waves constitute the periodic analogs of the bound states of a few dark solitons studied in Ref. [4]. In other words, a twin-atom or multiatom “soliton molecule” transforms into a one-dimensional “dark soliton crystal.”

The central issue behind the existence of families of dark-type sn waves is whether the binding energy of such “soliton crystals” is big enough to render them stable under propaga-

tion in the presence of random input perturbations. To address this issue we performed a rigorous linear stability analysis using a method specially suited to these types of solutions. The method of stability analysis for periodic wave patterns used here was introduced in Refs. [14,15] for the case of both  $\chi^{(2)}$  and  $\chi^{(3)}$  nonlinear media; thus here only the essential points necessary for discussion are recalled. We seek for perturbed solutions of Eqs. (1) in the form

$$q_{1,2}(\eta, \xi) = [w_{1,2}(\eta) + U_{1,2}(\eta, \xi) + iV_{1,2}(\eta, \xi)] \exp(ib_{1,2}\xi), \quad (7)$$

where  $U_{1,2}$  and  $V_{1,2}$  are the real and imaginary parts of the small perturbation, respectively. Such perturbations are represented in the spectral-type integral form:

$$U_{1,2}(\eta, \xi) = \text{Re} \left[ \int C(\delta) u_{1,2}(\eta, \delta) \exp(\delta\xi) d\delta \right], \quad (8)$$

$$V_{1,2}(\eta, \xi) = \text{Re} \left[ \int C(\delta) v_{1,2}(\eta, \delta) \exp(\delta\xi) d\delta \right],$$

where  $C(\delta)$  is the complex spectral amplitude and  $\delta$  is the complex growth rate of the perturbation. Substitution of expression (7) into Eqs. (1) and linearization yields the system of ordinary differential equations for the perturbation vector  $\Phi(\eta) = \{u_1, u_2, v_1, v_2, du_1/d\eta, du_2/d\eta, dv_1/d\eta, dv_2/d\eta\}^T$  and can be written in the matrix form:

$$\frac{d\Phi}{d\eta} = \mathcal{B}\Phi, \quad \mathcal{B} = \begin{pmatrix} \mathcal{O} & \mathcal{E} \\ \mathcal{N} & \mathcal{O} \end{pmatrix}, \quad (9)$$

$$\mathcal{N} = \begin{pmatrix} -2(b_1 - w_2)/d_1 & 2w_1/d_1 & -2\delta/d_1 & 0 \\ 4w_1/d_2 & -2b_2/d_2 & 0 & -2\delta/d_2 \\ 2\delta/d_1 & 0 & -2(b_1 + w_2)/d_1 & 2w_1/d_1 \\ 0 & 2\delta/d_2 & 4w_1/d_2 & -2b_2/d_2 \end{pmatrix},$$

where  $\mathcal{O}$  and  $\mathcal{E}$  are zero and unity  $4 \times 4$  matrices, respectively.

The general solution of Eqs. (9) is expressed in the matrix form  $\Phi(\eta) = \mathcal{I}(\eta, \eta') \Phi(\eta')$ . Here the Cauchy matrix  $\mathcal{I}(\eta, \eta')$  satisfies the initial value problem  $\partial \mathcal{I}(\eta, \eta') / \partial \eta = \mathcal{B}(\eta) \mathcal{I}(\eta, \eta')$ ,  $\mathcal{I}(\eta', \eta') = \mathcal{E}$ . The translation matrix of the perturbation eigenvector  $\Phi$  on one wave period  $T$  is expressed in terms of the Cauchy matrix  $\mathcal{P}(\eta) = \mathcal{I}(\eta + T, \eta)$ . The perturbation eigenvector  $\Phi_k(\eta)$  is finite along the  $\eta$  axis if the corresponding eigenvalue of the translation matrix  $|\lambda_k| = 1$  ( $k = 1, \dots, 8$ ). The eigenvalues  $\lambda_k$  are given by the roots of the characteristic polynomial

$$\det(\mathcal{P} - \lambda \mathcal{E}) = \sum_{k=0}^8 p_k \lambda^{8-k} = 0 \quad (10)$$

of the translation matrix, which is independent of  $\eta$ . The

coefficients of the polynomial can be written in terms of the traces  $T_k = \text{Tr}[\mathcal{P}^k(\eta)]$ , which are also independent of  $\eta$ . One finds that  $p_0 = 1$ ,  $p_1 = -T_1$ ,  $p_2 = (T_1^2 - T_2)/2$ ,  $p_3 = -T_1^3/6 + T_1 T_2/2 - T_3/3$ ,  $p_4 = T_1^4/24 - T_1^2 T_2/4 + T_1 T_3/3 + T_1^2/8 - T_4/4$ ,  $p_5 = p_3$ ,  $p_6 = p_2$ ,  $p_7 = p_1$ ,  $p_8 = p_0$ . Notice that four of the eight eigenvalues  $\lambda_k$  can be excluded, since it follows from the structure of the characteristic polynomial that  $\lambda_k = 1/\lambda_{k+4}$  ( $k = 1, \dots, 4$ ). One can show that the corresponding eigenvectors satisfy the symmetry relations  $\Phi_k(\eta) = \Phi_{k+4}(-\eta)$  ( $k = 1, \dots, 4$ ).

To elucidate the outcome of the stability analysis, we thoroughly scanned the complex increment half plane  $\text{Re}(\delta) \geq 0$  and analyzed the eigenvalues  $\lambda_k$ , looking for areas of existence of “allowed” perturbations (inside these areas one has  $|\lambda_k| = 1$ ) for fixed values of the propagation constant  $b_1$  and phase-mismatch parameter  $\beta$ . Then we searched for the maximal growth rates inside these areas and finally cal-

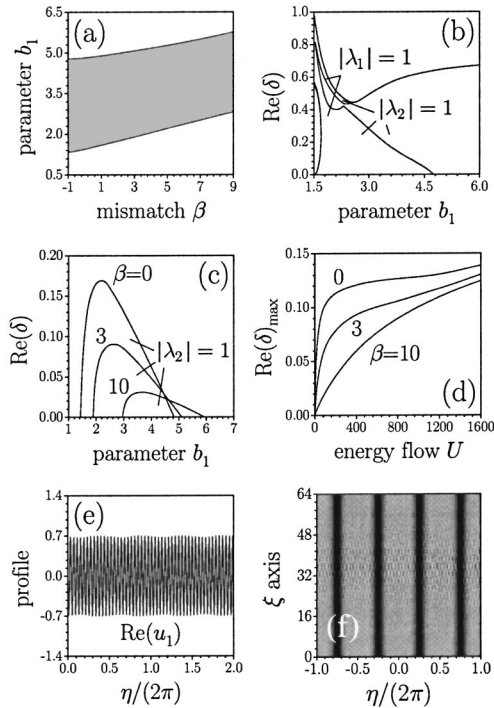


FIG. 2. (a) Area of existence of exponential instabilities for dark snoidal waves (shaded). Areas of existence of finite perturbations with real growth rates at  $\beta = -3$  (b) and 0, 3, 10 (c). (d) Maximum real part of complex growth rates versus energy flow for different phase mismatches. (e) One of the components of the perturbation corresponding to growth rate  $\delta = 0.0979 + 293.3921i$  and snoidal wave with  $b_1 = 7$  at  $\beta = 3$ . (f) Propagation of the snoidal wave in the presence of the perturbation depicted in (e). Only the FF wave is shown.

culated the corresponding perturbation modes. We emphasize that this requires an intense numerical effort.

There are two different types of instability of the dark periodic waves: “exponential” instabilities associated with purely real growth rates and “oscillatory” instabilities associated with complex growth rates. At  $\beta \leq -1$  snoidal-type waves were found to be exponentially unstable in the whole domain of their existence, whereas for  $\beta \geq -1$  exponential instabilities were found inside a certain relatively narrow band of propagation constants [see Fig. 2(a)]. The areas of existence of finite perturbations at negative and positive phase mismatches are shown in Figs. 2(b) and 2(c), respectively. Notice that at  $\beta \leq -1$  the instability growth rates are quite high and thus will lead to a fast decay of the corresponding wave in the whole range of its existence. The important result revealed in this paper is that at  $\beta \geq -1$  the situation drastically changes: While exponential instabilities are still possible in a narrow band of propagation constants [Fig. 2(c)], the maximal value of the corresponding growth rate inside these bands is very small compared with typical growth rates encountered when  $\beta \leq -1$ . Moreover, when the mismatch  $\beta$  increases, the maximum value of the growth rate inside the instability band quickly decreases. This is consistent with the suppression of exponential instabilities of snoidal waves in the large (and positive) phase-mismatch limit, i.e., an effective Kerr medium.

Therefore, on physical grounds the important implication is that near phase matching, which is the most interesting case experimentally, such a small growth rate of the exponential instabilities can manifest itself only after a long propagation distance, typically far larger than any feasible quadratic crystal length. Actually, the exact numerical simulations, discussed below, of the evolution of the perturbed stationary solutions for large propagation distances, beyond the regime where the predictions of linear stability hold, reveal that the growth of the perturbations does not even always lead to the eventual decay of the sn waves.

“Oscillatory” instabilities were found to exist for all energy levels and material parameters. At negative phase mismatches the oscillatory instability is strong and the real parts of the complex growth rates reach almost the same magnitude as those associated with exponential instabilities. However, at positive and zero phase mismatches the maximum positive value of the complex growth rates,  $\text{Re}(\delta)_{\text{max}}$ , associated with oscillatory instabilities was found to be quite small and to grow monotonically with the energy flow  $U$ . Notice that the band of energy flows where  $\text{Re}(\delta)_{\text{max}} \leq 0.05$  rapidly increases from  $0 \leq U \leq 62.2$  at  $\beta = 3$  to  $0 \leq U \leq 314$  at  $\beta = 10$ . Since the decay length of waves with such low increments is huge and exceeds feasible crystal lengths by several orders of magnitude, the important conclusion is that it should be possible to observe snoidal-type waves experimentally. Notice also that inside these intervals of “metastability” the contrast, energy sharing, integral width, and other characteristics of dark snoidal-type waves change considerably. In the limit  $\beta \rightarrow \infty$  the “metastability” region broadens and both oscillatory and exponential instabilities are suppressed. The last result is consistent with the stability of dark snoidal waves in the corresponding Kerr medium. The imaginary part of the complex growth rates rapidly increases as  $U \rightarrow \infty$ . We have found that dominant frequencies in the spectrum of perturbation with highest  $\text{Re}(\delta)$  can be estimated as  $\Omega \approx \pm [2 \text{Im}(\delta)]^{1/2}$  and at moderate and high energy flows are much higher than the frequencies of their own harmonics of snoidal waves. This means that in the case of well-localized high-energy waves the most “harmful” high-frequency perturbations lie far from the frequency band of snoidal waves and could potentially be removed by spectral filtering. For example, for a wave with  $b_1 = 7$  at  $\beta = 3$  the snoidal wave’s own frequency band is given by  $-8 \leq \Omega \leq 8$ , while the dominant frequencies in the perturbation spectrum are  $\Omega \approx \pm 24$  [see Fig. 2(e) which shows the profile of the perturbation for this wave]. A typical scenario of the instability development for the snoidal-type waves is shown in Fig. 2(f). One can clearly see the appearance of high-frequency modulations of the otherwise smooth profile; however, the depth of this modulation is small and does not lead to complete decay of the wave.

To confirm the results of the linear stability analysis and to elucidate the influence of an envelope on the snoidal wave propagation, we performed a set of simulations of Eqs. (1) with the input conditions  $q_{1,2}(\eta, 0) = w_{1,2}(\eta)G(\eta)[1 + \rho_{1,2}(\eta)]$ , where  $\rho_{1,2}(\eta)$  is a multiplicative Gaussian noise with variance  $\sigma_{1,2}^2$ , and  $G(\eta)$  is a wide envelope modulating the infinite periodic snoidal-type pattern. Notice that one of

the obvious consequences of the superimposed wide envelope is slow broadening of the discrete spectral lines (modes) forming a periodic wave pattern. We have found that in some cases (when the growth rates predicted by linear stability analysis are small enough) perturbed snoidal waves with low and moderate energy flows can survive up to 1000 propagation units, exceeding any feasible crystal length by several orders of magnitude (Fig. 3). The band of energy flows corresponding to such “metastable” propagation quickly increases with increase of the phase mismatch, as predicted by the stability analysis. As in the case of regular perturbations in linear stability analysis, in the case of random perturbations instability of high-energy waves manifests itself in the appearance of high-frequency oscillations and leads to behavior analogous to that depicted in Fig. 2(f).

In conclusion, we have numerically found periodic snoidal-type solutions describing phase-locked wave patterns in quadratic nonlinear media and presented their basic properties. The rigorous linear stability analysis of the solutions has shown the existence of parameter areas where these waves exhibit very weak instabilities; thus we termed them metastable. In such areas the growth rate of perturbations is small enough to allow structural stability of the perturbed waves during hundreds of propagation units. Such patterns of periodic pixel-like structures can find applications, e.g., in the study of complex light patterns generated by modulational instabilities, or in the implementation of digital image processing schemes based on solitonlike arrays [16,17], and in the formation of two-dimensional discrete solitons in mul-

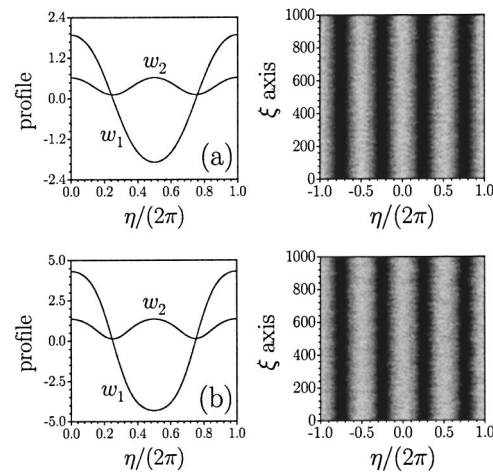


FIG. 3. (a) shows the profile of the stationary dark snoidal wave with  $b_1=1$  at  $\beta=3$  and its long-term propagation in the presence of white input noise superimposed on the stationary solution. (b) The same as in (a) but for the wave with  $b_1=1.6$  and  $\beta=10$ . Noise variance  $\sigma_{1,2}^2=0.01$ . Only the FF wave is shown.

ticolor photonic lattices (see [18] for a photorefractive counterpart).

Financial support from CONACyT under Grant No. U39681-F is gratefully acknowledged by V.A.V. Y.V.K. and L.T. acknowledge support by the Generalitat de Catalunya and by the Spanish Government under Contract No. BFM2002-2861.

- 
- [1] M. J. Werner and P. D. Drummond, *Opt. Lett.* **19**, 613 (1994).  
 [2] C. R. Menyuk, R. Schiek, and L. Torner, *J. Opt. Soc. Am. B* **11**, 2434 (1994).  
 [3] K. Hayata and M. Koshiba, *Phys. Rev. A* **50**, 675 (1994).  
 [4] A. V. Buryak and Y. S. Kivshar, *Phys. Rev. A* **51**, R41 (1995); *Opt. Lett.* **20**, 834 (1995); *Phys. Lett. A* **197**, 407 (1995).  
 [5] H. He, M. J. Werner, and P. D. Drummond, *Phys. Rev. E* **54**, 896 (1996).  
 [6] V. M. Agranovich, S. A. Darmanyan, A. M. Kamchatnov, T. A. Leskova, and A. D. Boardman, *Phys. Rev. E* **55**, 1894 (1997).  
 [7] A. R. Chapman, B. A. Malomed, J. Yang, and D. J. Kaup, *Physica D* **152**, 340 (2001).  
 [8] G. I. Stegeman, D. J. Hagan, and L. Torner, *Opt. Quantum Electron.* **28**, 1691 (1996).  
 [9] A. V. Buryak, P. Di Trapani, D. V. Skryabin, and S. Trillo, *Phys. Rep.* **370**, 63 (2002).  
 [10] D. F. Parker, *J. Opt. Soc. Am. B* **15**, 1061 (1998).  
 [11] P. Ferro and S. Trillo, *Phys. Rev. E* **51**, 4994 (1995).  
 [12] S. Laforune, P. Winternitz, and C. R. Menyuk, *Phys. Rev. E* **58**, 2518 (1998).  
 [13] Y. V. Kartashov, V. A. Vysloukh, and L. Torner, *Phys. Rev. E* **67**, 066612 (2003).  
 [14] Y. V. Kartashov, A. A. Egorov, A. S. Zelenina, V. A. Vysloukh, and L. Torner (unpublished).  
 [15] Y. V. Kartashov, V. A. Aleshkevich, V. A. Vysloukh, A. A. Egorov, and A. S. Zelenina, *Phys. Rev. E* **67**, 036613 (2003); *J. Opt. Soc. Am. B* **20**, 1273 (2003).  
 [16] A. Bramati, W. Chinaglia, S. Minardi, and P. Di Trapani, *Opt. Lett.* **26**, 1409 (2001).  
 [17] S. Minardi, G. Arrighi, P. Di Trapani, A. Varanavicius, and A. Piskarskas, *Opt. Lett.* **27**, 2097 (2002).  
 [18] J. W. Fleischer, M. Segev, N. K. Efremidis, and D. N. Christodoulides, *Nature (London)* **422**, 147 (2003).